PAPER • OPEN ACCESS

Attosecond control of spin polarization in electron–ion recollision driven by intense tailored fields

To cite this article: David Ayuso *et al* 2017 *New J. Phys.* **19** 073007

New Journal of Physics
The open access journal at the forefront of physics

Deutsche Physikalische Gesellschaft DPG
IOP Institute of Physics

Published in partnership with: Deutsche Physikalische Gesellschaft and the Institute of Physics

OPEN ACCESS

RECEIVED
14 December 2016

ACCEPTED FOR PUBLICATION
15 May 2017

PUBLISHED
6 July 2017

PAPER

Attosecond control of spin polarization in electron–ion recollision driven by intense tailored fields

David Ayuso[1], **Alvaro Jiménez-Galán**[1], **Felipe Morales**[1], **Misha Ivanov**[1,2,3] **and Olga Smirnova**[1,4]

[1] Max-Born Institute for Nonlinear Optics and Short Pulse Spectroscopy, Max-Born-Straße 2A, D-12489 Berlin, Germany
[2] Department of Physics, Imperial College London, South Kensington Campus, SW72AZ London, United Kingdom
[3] Institute für Physik, Humboldt-Universität zu Berlin, Newtonstraße 15, D-12489 Berlin, Germany
[4] Technische Universität Berlin, Ernst-Ruska-Gebäude, Hardenbergstraße 36A, D-10623 Berlin, Germany

E-mail: olga.smirnova@mbi-berlin.de

Keywords: spin polarization, attosecond physics, strong laser fields, electron–ion recollision

Abstract

Tunnel ionization of noble gas atoms driven by a strong circularly polarized laser field in combination with a counter-rotating second harmonic generates spin-polarized electrons correlated to the spin-polarized ionic core. Crucially, such two-color field can bring the spin-polarized electrons back to the parent ion, enabling the scattering of the spin-polarized electron on the spin-polarized parent ion. Here we show how one can control the degree of spin polarization as a function of electron energy and recollision time by tuning the laser parameters, such as the relative intensities of the counter-rotating fields. The attosecond precision of the control over the degree of spin polarization opens the door for attosecond control and spectroscopy of spin-resolved dynamics.

1. Introduction

Electron spin governs the behavior of matter, arranging the electronic shells of the elements in the periodic table through the Pauli exclusion principle [1], in particular giving rise to magnetism [2]. Not surprisingly, the generation of spin-polarized electrons [3] has been an important research topic for many decades. One well-established method [4], suggested by Fano, relies on single-photon ionization of atoms, with the photon energy tuned to the Cooper minimum in photoionization. This scheme [4] has been extended to the case of few-photon ionization in the perturbative light-atom interaction regime in [5–7], with special attention paid to the role of intermediate resonances.

The study of spin polarization during strong-field ionization in the highly non-perturbative regime of laser-atom interaction [8–10] demonstrated that careful tuning of the laser photon energy in resonance with a specific intermediate state, or into the Cooper minimum, becomes completely unnecessary for sufficiently high laser intensities. In intense circularly polarized laser fields, spin-polarized electrons are generated almost by default, as long as there is sufficient spin-orbit splitting in the ionic ground state and the electron is removed from an orbital with angular momentum $l \geqslant 1$.

This effect results from the interplay of several factors. The first is the unusual propensity rule in strong-field ionization [8]: electrons that counter-rotate with the field ionize more easily than the co-rotating electrons [11]. This means different ionization rates for p_- ($l_z = m = -1$) and p_+ ($l_z = m = +1$) electrons in noble gases [11–16] and diatomic molecules [17] and a preference for the orientation of the orbital angular momentum in the created ion. The second is the spin-orbit interaction (and splitting) in the ionic ground state. It couples angular-momentum sensitivity of strong-field ionization to the spin, and it also ensures that the continuum electrons correlated to the different final ionic states can be distinguished. The third is the correlation between the spin of the continuum electron and the spin of the hole left in the parent atom. For example, if the ion of a noble gas atom such as xenon is created in the $^2P_{1/2}$ state, the spin of the hole must be anti-parallel to its angular momentum. Both are equal to the initial values for the liberated electron. Hence, if the liberated electron had its original $l_z = m = -1$ (which is preferred), the hole will have $L_z = -1$, its spin must then be $+1/2$, and hence

the spin of the liberated electron will have the positive projection on the quantization axis. The case of $l_z = +1$ is, of course, also possible, but less likely.

Strictly speaking, the correlation between the continuum electron and the hole, i.e. the state of the ion, is beyond classical: the generated wavefunction describes the entangled electron-hole state. Even for a given ionic state, e.g. $^2P_{1/2}$, the ion can be left with the spin of the hole both parallel and anti-parallel to the quantization axis, yielding $|\Psi_{eh}\rangle = a|\uparrow_e, \uparrow_h\rangle + b|\downarrow_e, \downarrow_h\rangle$. Here a, b are the complex amplitudes defining the phase between the different components of the entangled electron–ion wavefunction. However, the calculation of the spin-polarized currents correlated to different final states of the ion shows that this phase drops out from the result [8], unless transitions in the ion are induced. The quantum aspect of electron–ion correlation will manifest, however, in the case of spin-changing and/or inelastic recollisions, which will leave the ion in the same final state after the recollision but will have different intermediate spin-polarized electron–ion states before it. It will also matter for radiative electron–hole recombination—the process responsible for high harmonic generation—which will bring the two parts of the full wavefunction to the same final state. The quantum nature of electron–ion correlation also manifests in the anti-symmetrization of the full wavefunction, which affects exchange contribution to re-scattering and significantly impacts such processes as recollision-driven non-sequential double ionization [18].

The possibility of inducing recollision of spin-polarized electrons with the parent ion can open new directions in attosecond spectroscopy [9, 10]. A numerical analysis indicating the possibility of producing electron–ion recollision with spin-polarized electrons using elliptically polarized single-color laser fields was presented in [10]. Not surprisingly, the degree of spin polarization is higher for higher ellipticity of the ionizing field. The flip side of the coin, however, is that high ellipticity of the ionizing field reduces the chance of electron return to the parent ion. In this context, the use of an intense circularly polarized laser field in combination with its counter-rotating second harmonic, known as a bi-circular field, constitutes a powerful tool for introducing the spin degree of freedom into attosecond science, due to the opportunity to combine circular polarization with efficient recollision offered by these fields [9, 19–23, 44, 45]. The application of bi-circular fields can lead to the production of ultrashort circularly and elliptically polarized laser pulses in the XUV domain [22–28]. Their chiral nature offers unique possibilities for probing molecular chirality [29] or symmetry breaking [30] at their natural time scales via high harmonic generation spectroscopy.

Recent theoretical work [9] has shown that bi-circular fields can produce spin-polarized electrons. An analysis of ATI spectra of xenon atoms revealed that both direct and re-scattered electrons are spin-polarized, with polarization changing as a function of the final electron momentum. Several key questions, however, remained unanswered. Why does spin polarization change for different final electron momenta in the high-energy region of the spectrum, and what determines this change? Is it possible to control spin polarization, in particular its rapid oscillations across the spectrum? How do the parameters of the bi-circular field affect spin polarization at the moment of recollision? What about the temporal dimension? How does the spin polarization of the recolliding current change as a function of time? Answering these questions is essential if we aim to bring the spin dimension into time-resolved collisions. The generation of recolliding electron currents with tunable degree of spin polarization on the sub-femtosecond time-scale will bring new opportunities for probing spin or chiral dynamics in matter.

Here we present a detailed theoretical study of spin polarization in electron–core recollision driven by bi-circular fields, emphasizing the possibilities for, and the physical mechanisms of controlling the degree of spin-polarization by changing the parameters of the bi-circular field. The paper provides answers for the questions posed in the previous paragraph and is organized as follows. Section 2 describes the theoretical approach. Section 3 describes our results, focusing on the analytical analysis of how the properties of the quantum electron trajectories define the spin polarization. This allows us to establish the origin of spin polarization in bi-circular fields (section 3.1) and show how to achieve its attosecond control by tailoring the laser fields (section 3.2). Section 4 concludes the paper.

2. Method

Consider ionization, followed by electron–parent ion recollision, of xenon atoms driven by a strong right circularly polarized field in combination with the counter-rotating second harmonic. The resulting electric field can be written, in the dipole approximation, as:

$$\mathbf{F}(t) = [F_{0,\omega}\cos(\omega t) + F_{0,2\omega}\cos(2\omega t)]\hat{\mathbf{x}} + [F_{0,\omega}\sin(\omega t) - F_{0,2\omega}\sin(2\omega t)]\hat{\mathbf{y}}, \quad (1)$$

where $F_{0,\omega}$ and $F_{0,2\omega}$ are the amplitudes of the right and left circularly polarized fields, respectively, with frequencies ω and 2ω. Within the strong-field approximation, the continuum electron wavefunction at time t is given by [31]:

$$|\Psi(t)\rangle = \mathrm{i}\int_{t_0}^{t} \mathrm{d}t' \mathrm{e}^{\mathrm{i}\mathrm{IP}(t'-t_0)}\mathbf{F}(t') \int \mathrm{d}\mathbf{p}\ \mathrm{d}(\mathbf{p}+\mathbf{A}(t'))\ |\mathbf{p}+\mathbf{A}(t)\rangle_V, \tag{2}$$

where IP is the ionization potential, $\mathbf{p}$ is the drift (canonical) momentum, related to the the kinetic momentum $\mathbf{k}(t)$ by $\mathbf{k}(t) = \mathbf{p} + \mathbf{A}(t)$, $\mathbf{d}(\mathbf{p}+\mathbf{A}(t)) = \langle \mathbf{p}+\mathbf{A}(t)|\hat{\mathbf{d}}|\Psi_0\rangle$ is the transition dipole matrix element from the initial ground state $|\Psi_0\rangle$ (the system is assumed to be in the ground state at $t = t_0$) to a Volkov state $|\mathbf{p}+\mathbf{A}(t)\rangle_V$, given by

$$|\mathbf{p}+\mathbf{A}(t)\rangle_V = \frac{1}{(2\pi)^{3/2}} \mathrm{e}^{-\mathrm{i}S_V(t,t',\mathbf{p})} \mathrm{e}^{\mathrm{i}[\mathbf{p}+\mathbf{A}(t)]\cdot\mathbf{r}}, \tag{3}$$

where $S_V(t,\ t',\ \mathbf{p})$ is the Volkov phase:

$$S_V(t,\ t',\ \mathbf{p}) = \frac{1}{2}\int_{t'}^{t} \mathrm{d}\tau\,[\mathbf{p}+\mathbf{A}(\tau)]^2. \tag{4}$$

Equation (2) can be used to calculate different observables, such as photoelectron yields, induced polarization and harmonic spectra [31]. Here we are interested in analyzing the degree of spin polarization of the electrons that are driven back to the ionic core. This requires a measure of the recollision probability, resolved on the state of the ion and on the spin of the returning electron. The latter is determined by the initial magnetic quantum number of the state from which the electron tunnels and the state of the ion that has been created upon ionization, as described in [8]. As for the recollision probability, given that the size of the returning wave packet far exceeds the size of the atom, an excellent measure of the recollision amplitude is the projection of the continuum wavefunction (equation (2)) $|\Psi(t)\rangle$ on any compact object at the origin; the recollision current will scale with the object area. To obtain the required recollision probability density at the origin, we simply project $|\Psi(t)\rangle$ on the delta-function at the origin, yielding

$$a_{\mathrm{rec}}(t) = \frac{\mathrm{i}}{(2\pi)^{3/2}}\int_{t_0}^{t} \mathrm{d}t'\mathbf{F}(t') \int \mathrm{d}\mathbf{p}\ \mathrm{d}(\mathbf{p}+\mathbf{A}(t'))\ \mathrm{e}^{-\mathrm{i}[S_V(t,t',\mathbf{p})+\mathrm{IP}(t-t')]}. \tag{5}$$

The degree of spin polarization of the recolliding electrons as a function of the recollision time t is given by the normalized difference between the recollision probability densities for electrons recolliding with spin up ($w_\uparrow(t) = |a_\uparrow(t)|^2$) and spin down ($w_\downarrow(t) = |a_\downarrow(t)|^2$) [8]:

$$\mathrm{SP}(t) = \frac{w_\uparrow(t) - w_\downarrow(t)}{w_\uparrow(t) + w_\downarrow(t)}. \tag{6}$$

The densities $w_\uparrow(t)$ and $w_\downarrow(t)$ are obtained from the recollision densities $w^{p_+,p_-}_{\mathrm{IP}^{2}P_{3/2,1/2}}(t) = |a^{p_+,p_-}_{\mathrm{IP}^{2}P_{3/2,1/2}}(t)|^2$ correlated to ionization from the p_+ and p_- orbitals, resolved on the ionic states $^2P_{3/2}$ and $^2P_{1/2}$, and the corresponding Clebsch–Gordan coefficients [8]:

$$w_\uparrow(t) = w^{p_+}_{\mathrm{IP}^{2}P_{3/2}}(t) + \frac{2}{3}w^{p_-}_{\mathrm{IP}^{2}P_{1/2}}(t) + \frac{1}{3}w^{p_-}_{\mathrm{IP}^{2}P_{3/2}}(t), \tag{7}$$

$$w_\downarrow(t) = w^{p_-}_{\mathrm{IP}^{2}P_{3/2}}(t) + \frac{2}{3}w^{p_+}_{\mathrm{IP}^{2}P_{1/2}}(t) + \frac{1}{3}w^{p_+}_{\mathrm{IP}^{2}P_{3/2}}(t). \tag{8}$$

The contribution of the p_0 orbital is negligible [11, 13]. The key quantities in these expressions are the recollision densities resolved on the initial orbital and the final ionic state, $w^{p_-}_{\mathrm{IP}^{2}P_{1/2}} = |a^{p_-}_{\mathrm{IP}^{2}P_{1/2}}|^2$, etc. Application of the saddle point method (see e.g. [31]) to the integral equation (5) allows us to perform the semi-classical analysis of this expression in terms of electron trajectories, getting insight into the physical origin of spin polarization during recollision. The saddle points are calculated by solving the following set of equations [31]:

$$\frac{[\mathbf{p}+\mathbf{A}(t_\mathrm{i})]^2}{2} + \mathrm{IP} = 0, \tag{9}$$

$$\int_{t_\mathrm{i}}^{t_\mathrm{r}} \mathrm{d}\tau\,[\mathbf{p}+\mathbf{A}(\tau)] = 0, \tag{10}$$

where IP is the ionization potential, t_i and t_r are the complex ionization and recollision times, respectively. Equation (9) describes tunneling and equation (10) requires that the electron returns to the core.

Figure 1 shows a schematic representation of the process on the complex time plane. The electron enters the barrier at complex time $t_\mathrm{i} = t_\mathrm{i}' + \mathrm{i}t_\mathrm{i}''$. The motion in the classically forbidden region occurs along the imaginary time axis and the electron is born in the continuum at real time t_i'. As a result, the recollision time t_r and the canonical momentum $\mathbf{p}$ are, in general, complex. To further simplify the analysis, we can take into account that for most of the relevant trajectories the imaginary part of their recollision time is rather small. This allows one to keep the recollision time on the real time axis, also simplifying the treatment of the usual divergences near the cutoff region, see [31]. Setting t_r then defines $\mathbf{p}$ and t_i from equations (9) and (10).

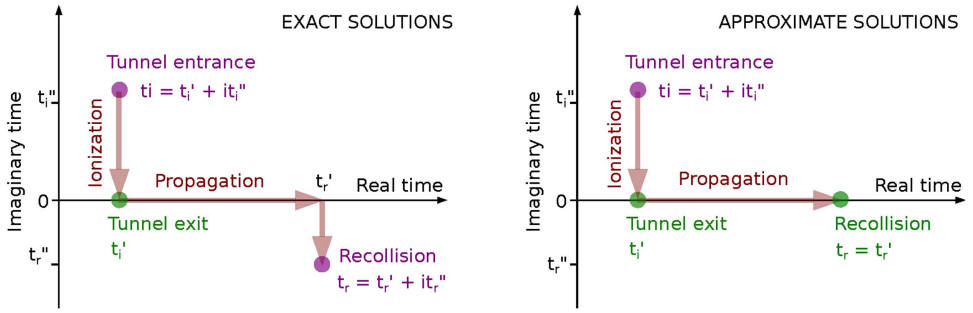

Figure 1. Schematic representation of the contour time integration of the action. Ionization starts at a complex time $t_i = t_i' + it_i''$, the electron tunnels out of the potential barrier at the real time t_i', and returns to the ionic core at $t_r = t_r' + it_r''$ (left panel). If the imaginary part of the recollision time is sufficiently small, one can keep the recollision time on the real time axis (right panel), simplifying the treatment of the cutoff region.

The recollision densities correlated to ionization from p_+ and p_- orbitals are proportional to:

$$w_{\mathrm{IP}}^{p_m} \propto |\mathrm{e}^{-\mathrm{i}[S_V(t_r,t_i,\mathbf{p})+\mathrm{IP}(t_r-t_i)]+\mathrm{i}m\phi_{\mathbf{k}(t_i)}}|^2 \simeq \mathrm{e}^{2\Im\{S_V(t_i',t_i,\mathbf{p})\}-2\mathrm{IP}t_i''}\ \mathrm{e}^{-2m\Im\{\phi_{\mathbf{k}(t_i)}\}}. \tag{11}$$

In this expression, the first key quantity that determines the magnitude of $w_{\mathrm{IP}}^{p_m}$ is the imaginary part of action. It is mostly accumulated between the times $t_i = t_i' + \mathrm{i}t_i''$ and t_i', i.e. in the classically forbidden region. The second key quantity, which depends on the projection m of the angular momentum, is the complex-valued ionization angle $\phi_{\mathbf{k}(t_i)}$. It is given by the following expression:

$$\phi_{\mathbf{k}(t_i)} = \mathrm{atan}\left(-\frac{k_x'(t_i)}{k_y'(t_i)}\right) + \mathrm{i}\ \mathrm{atanh}\left(\frac{k_x'(t_i)}{k_y''(t_i)}\right) \tag{12}$$

with $k_x(t_i) = k_x'(t_i) + \mathrm{i}k_x''(t_i)$ and $k_y(t_i) = k_y'(t_i) + \mathrm{i}k_y''(t_i)$ being the complex velocities along x and y directions, respectively.

Note that the difference between the recollision densities from p_+ and p_- orbitals depends solely on the imaginary part of the ionization angle, since the action is the same in both cases. The ratio of these recollision densities, which fully determines the spin polarization of the recollision current, is therefore given by a very simple analytical expression

$$w_{\mathrm{IP}}^{p_-}/w_{\mathrm{IP}}^{p_+} = \mathrm{e}^{4\Im\{\phi_{\mathbf{k}(t_i)}\}}. \tag{13}$$

Note also that this expression is not limited to the case of two circular counter-rotating fields, but applies to any combination of light frequencies and polarizations, i.e. to an arbitrary vector potential $\boldsymbol{A}(t)$. It allows one to easily evaluate how tailoring the laser field controls spin polarization at the moment of recollision. Here, we focus on the bi-circular case of the counter-rotating ω, 2ω fields.

Finally, the electron recollision energy is calculated as

$$E_{\mathrm{rec}} = \frac{[\mathbf{p} + \boldsymbol{A}(t_r)]^2}{2}. \tag{14}$$

For approximate analysis which keeps the return time on the real axis, we neglect the small imaginary contribution to E_{rec}.

3. Results

The Lissajous curves of the electric field considered here (see equation (1)) and of the corresponding vector potential $\mathbf{A}(t)$, given by $\mathbf{F}(t) = -\mathrm{d}\mathbf{A}(t)/\mathrm{d}t$, are shown in figure 2, as well as the ionization and the recollision time windows (the field parameters are given in the figure 2 caption). The resulting electric field has a three-fold symmetry, with 3 peaks per cycle oriented at angles 0, $2\pi/3$ and $4\pi/3$ rad in the xy plane. Ionization is more likely to occur near the maxima of the electric field, where the tunneling barrier is thinner. Electrons liberated just before these maxima are unlikely to return to the core, those released after the maximum can recollide.

Consider strong-field ionization of a xenon atom from the outermost 5p shell. The spin-orbit interaction splits the energy levels of the ion into $^2P_{3/2}$ and $^2P_{1/2}$, with ionization potentials $\mathrm{IP}^{^2P_{3/2}} = 12.13$ eV and $\mathrm{IP}^{^2P_{1/2}} = 13.43$ eV . Our calculations considered both ionic states, as needed for calculating spin polarization. The saddle point equations (equations (9) and (10)) have been solved numerically, allowing the ionization and return times to be complex (exact solutions), and also by keeping the return time on the real time axis (approximate solutions), as represented in figure 1. The real and imaginary parts of the ionization time, the

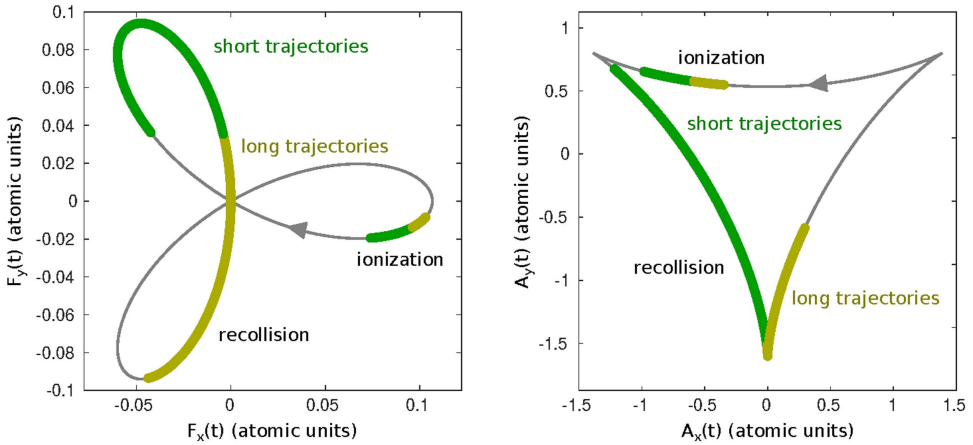

Figure 2. Electric field (left panel) and vector potential (right panel) resulting from combining a RCP field of frequency $\omega = 0.05$ a.u. and intensity $I = 10^{14}$ W cm^{-2} with a LCP field of frequency 2ω and equal intensity. The ionization and recollision time-windows are indicated in the figures for short (green) and long (yellow) trajectories for one of the three ionization bursts.

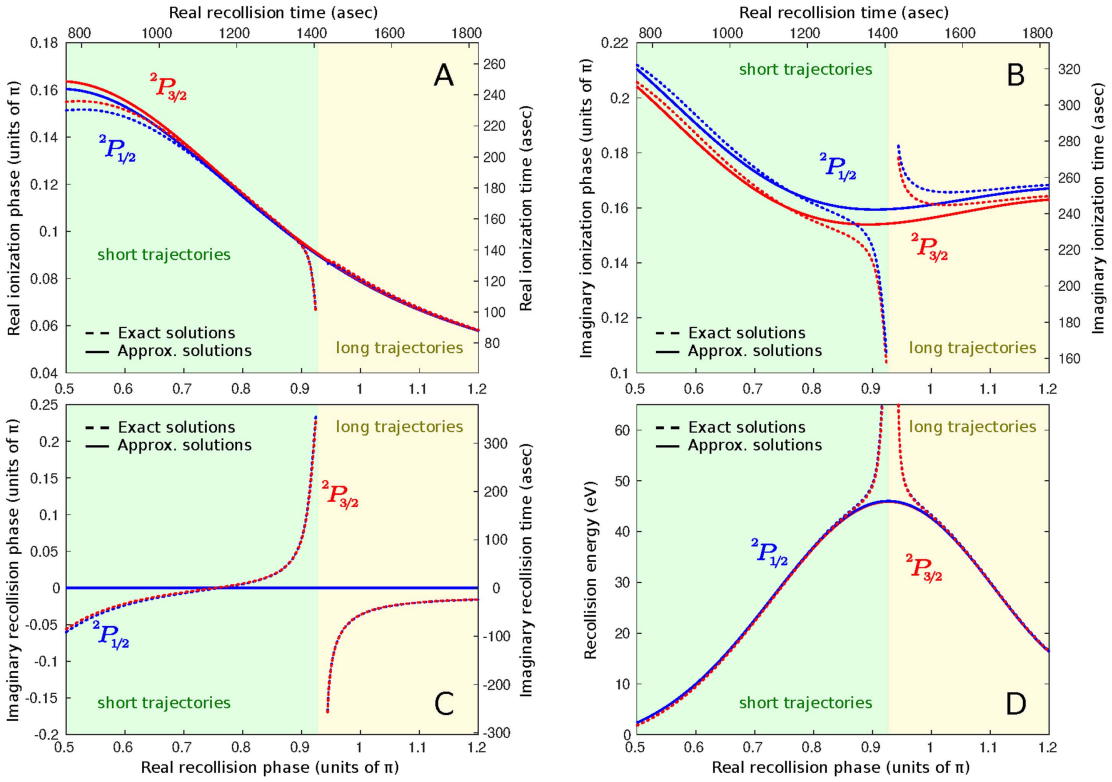

Figure 3. Saddle point solutions for the bi-circular field represented in figure 2 as functions of the real part of the recollision time: real (A) and imaginary (B) parts of the ionization time, imaginary part of the recollision time (C), and recollision energy (D). Full saddle points (dashed lines) have been calculated allowing both ionization and recollision times to be complex, whereas approximate solutions (full lines) have been obtained by keeping the time of return on the real time axis (see figure 1). Results are shown for the ionic states of xenon $^2P_{3/2}$ (red lines) and $^2P_{1/2}$ (blue lines), with ionization potentials $\mathrm{IP}^{^2P_{3/2}} = 12.13$ eV and $\mathrm{IP}^{^2P_{1/2}} = 13.43$ eV.

complex part of the recollision time and the recollision energy (evaluated using equation (14)) are shown in figure 3, as functions of the real part of the return time. Our exact solutions agree with those reported previously in [21] and the approximate solutions agree well with the exact ones. We can see that the imaginary part of the recollision time (figure 3(c)) is rather small, except near the cutoff, where the saddle point method diverges. The main advantage of using approximate solutions and keeping the recollision time on the real time axis is that the ionization time and the recollision energy behave smoothly in the vicinity of the cutoff, while being very similar to the exact solutions outside this region.

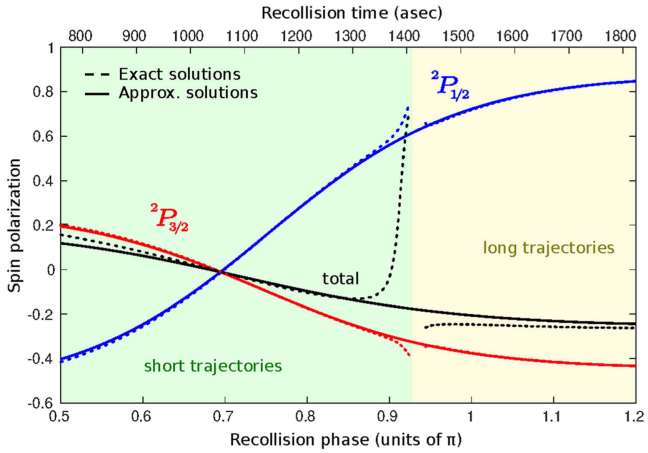

Figure 4. Total spin polarization (black lines) and spin polarization resolved in the $^2P_{3/2}$ (red lines) and in the $^2P_{1/2}$ (blue lines) states of the core as a function of the recollision time. Spin polarization has been calculated using the exact (full lines) and the approximate (dashed lines) saddle points solutions shown in figure 3.

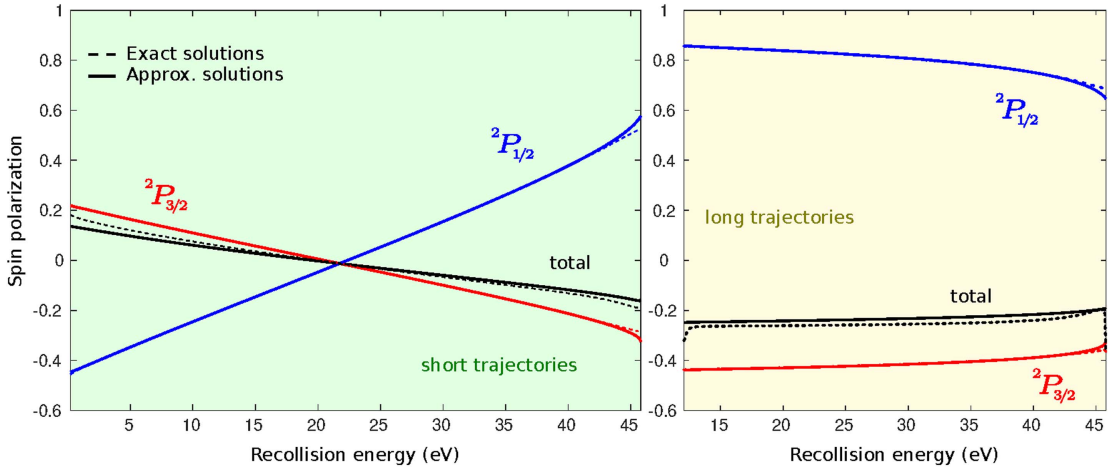

Figure 5. Total spin polarization (black lines) and spin polarization resolved in the $^2P_{3/2}$ (red lines) and in the $^2P_{1/2}$ (blue lines) states of the core as a function of the recollision energy for short (left panel) and long (right panel) trajectories. Spin polarization has been calculated using the exact (full lines) and the approximate (dashed lines) saddle points solutions shown in figure 3.

Let us compare now the results for the states $^2P_{3/2}$ and $^2P_{1/2}$ of the ion. As expected, the real part of the ionization time (figure 3(a)) and the recollision energy (figure 3(c)) are almost identical in both cases. The imaginary part of the ionization time, however (figure 3(b)), is slightly smaller for the $^2P_{3/2}$ state, with the lower IP, resulting in higher ionization amplitudes.

We have evaluated the degree of spin polarization in recollision (equation (6)) using the saddle point solutions shown in figure 3 and equation (13). Total spin polarization is shown in figure 4 as a function of the recollision time, together with the degree of polarization resolved in the $^2P_{1/2}$ and $^2P_{3/2}$ states of the core. It is clear from the figure that recolliding electrons are spin-polarized and that their degree of polarization depends strongly on the recollision time. Electrons that return to the core at earlier (later) times are more likely to have spin up (down). Note also that spin polarization resolved in the ionic states $^2P_{1/2}$ and $^2P_{3/2}$ has opposite sign. Both spin polarization resolved on the states of the ion and the total spin polarization change sign at the recollision phase (time) of 0.7π rad (1.11 fsec). Each return time is associated with a given recollision energy, which is the well-known time–energy mapping [31] (see figure 3(d)). Figure 5 shows spin polarization as a function of the recollision energy for short and long trajectories. Whereas for the short trajectories spin polarization changes dramatically as a function of the recollision energy, for the long trajectories the variation is rather smooth.

The results presented in this section are consistent with those reported in [9] and [10]. We note that the values of spin polarization predicted in [9] by analyzing ATI spectra of xenon atoms seem to be much lower that the ones shown here. This apparent discrepancy is due to the different definition of the asymmetry parameter employed in [9] to quantify spin polarization.

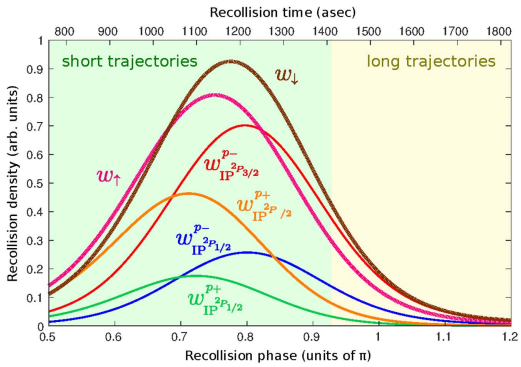

Figure 6. Recollision densities for p_+ and p_- electrons correlated to the states of the ion $^2P_{3/2}$ and $^2P_{1/2}$ as a function of the recollision time (thin lines) and total recollision densities for electrons with spin up and spin down (thick lines), calculated using the approximate quantum orbits resulting from keeping the time of return on the real time axis.

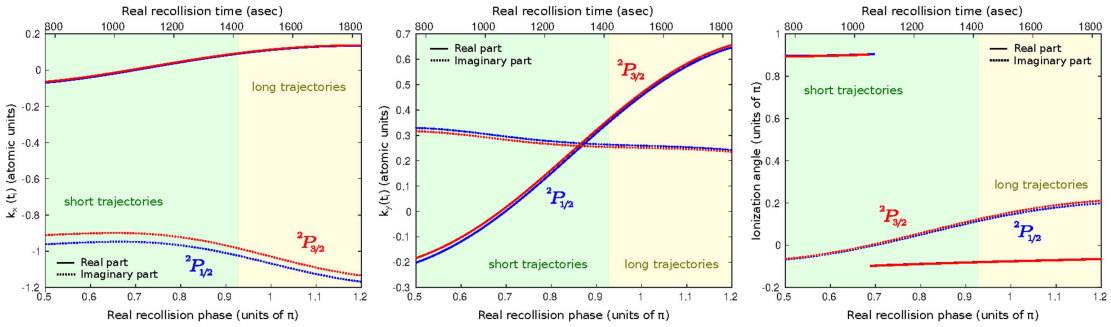

Figure 7. Real (full lines) and imaginary (dashed lines) parts of the electron velocity at $t = t_i$ (when it enters the classically forbidden region) along the x (left panel) and the y (central panel) directions, and ionization angle (right panel) calculated using equation (12), as a function of the recollision time.

3.1. Origin of spin polarization

To better understand the physical origin of spin polarization in recollision, let us analyze the recollision densities for different ionic channels. These are presented in figure 6 as a function of the recollision time, as well as the total recollision densities corresponding to electrons with spin up and spin down (equations (7) and (8)). There are three important things worth noting here. First, the recollision densities correlated to the $^2P_{3/2}$ state of the core ($w^{p_-}_{\mathrm{IP}^{2P_{3/2}}}$ and $w^{p_+}_{\mathrm{IP}^{2P_{3/2}}}$) are higher than those for the $^2P_{1/2}$ state ($w^{p_-}_{\mathrm{IP}^{2P_{1/2}}}$ and $w^{p_+}_{\mathrm{IP}^{2P_{1/2}}}$) because the lower ionization potential of this ionic state leads to smaller imaginary ionization times (see figure 3(b))—the tunneling barrier is thinner. Second, all recollision densities exhibit a maximum value that arises at lower recollision times in the case of the p_+ orbital ($w^{p_+}_{\mathrm{IP}^{2P_{3/2}}}$ and $w^{p_+}_{\mathrm{IP}^{2P_{1/2}}}$). Third, the densities resolved on the $^2P_{3/2}$ and $^2P_{1/2}$ states of the core cross at $\phi_r = 0.69\pi$ rad ($t_r = 1044$ asec) and $\phi_r = 0.70$ rad ($t_r = 1061$ asec), respectively, leading to changes of sign in spin polarization (see figure 4). In order to understand these features, we have examined the saddle point solutions at $t = t_i$, when the electron enters the classically forbidden region. The ionization velocity and the ionization angle are shown in figure 7 as a function of the recollision time. We can see that, for a recollision phase (time) of 0.7π rad (1.11 fsec), the real part of the ionization angle presents a jump of π and its imaginary component becomes zero. A purely real ionization angle leads to equal tunneling probabilities for p_+ and p_- orbitals (see equation equation (13)) and thus no spin polarization.

The time-dependent sensitivity of the recollision densities to the sense of rotation of the electron in its initial state can be understood by examining different quantum trajectories. Figure 8 contains a representation of the values of the electric field and the ionization velocity at $t = t_i$ of three quantum orbits that recollide with the $^2P_{3/2}$ state of the ion at different times: $\phi_r = 0.65\pi$ rad (positive spin polarization), $\phi_r = 0.69\pi$ rad (no spin polarization) and $\phi_r = 0.75\pi$ rad (negative spin polarization), calculated by keeping the time of return on the real time axis. We will refer to them as trajectories A, B, and C, respectively. The three trajectories have similar values of $\mathbf{k}''(t_i)$ and $\mathbf{F}(t_i)$. However, their values of $\mathbf{k}'(t_i)$ are very different.

Let us analyze the motion of the electron through the classically forbidden region, which occurs in imaginary time (see figure 1) and along the complex plane of spatial coordinates ($\mathbf{r} = \mathbf{r}' + i\mathbf{r}''$). The real part of the trajectory

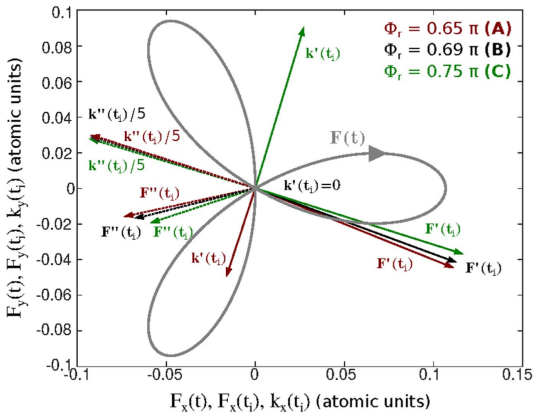

Figure 8. Real and imaginary parts of the kinetic momentum $\mathbf{k}(t_i)$ and the electric field $\mathbf{F}(t_i)$ at the saddle point of ionization $t = t_i$ for the quantum orbits that recollide with the core at $\phi_r = 0.65\pi$ rad (traj. A, red lines), $\phi_r = 0.69\pi$ (traj. B, black lines) and $\phi_r = 0.75\pi$ (traj. C, green lines); $\mathbf{k}(t_i) = \mathbf{k}'(t_i) + i\mathbf{k}''(t_i)$ and $\mathbf{F}(t_i) = \mathbf{F}'(t_i) + i\mathbf{F}''(t_i)$. Solutions are shown for one ionization burst. The electric field considered here, resulting from combining a RCP field of frequency $\omega = 0.05$ a.u. and intensity $I = 10^{14}$ W cm^{-2} with a counter-rotating second harmonic of equal intensity, is represented in the figure.

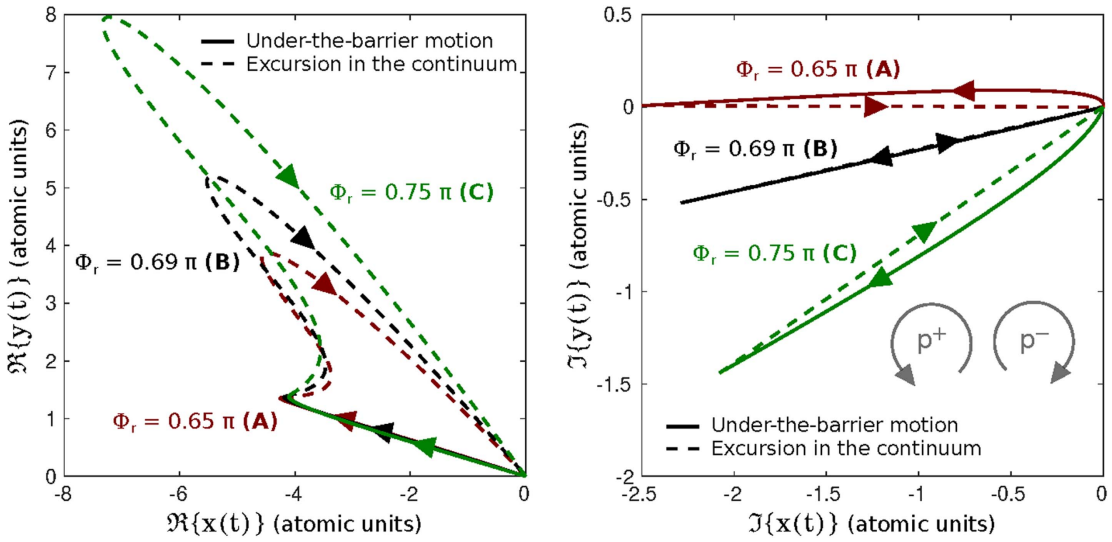

Figure 9. Real (left panel) and imaginary (right panel) components of the quantum orbits that recollide with the core at $\phi_r = 0.65\pi$ rad (traj. A, red lines), 0.69π rad (traj. B, black lines) and 0.75π rad (traj. C, green lines). Full lines: under-the-barrier motion, that is, electron motion in the classically forbidden region (see figure 1); dashed lines: excursion in the continuum. The corresponding recollision times ($t_r = \phi_r/\omega$) are $t_r = 314$, 334 and 363 asec. For illustration purposes, the sense of rotation of electrons in p_+ and p_- orbitals is depicted in the right panel.

depends on $\mathbf{k}''$ and $\mathbf{F}'$ according to $\mathbf{k}'' = \mathrm{d}\mathbf{r}'/\mathrm{d}\tau$ and $\mathbf{F}' = \mathrm{d}\mathbf{k}''/\mathrm{d}\tau$, with τ being the complex time variable. Under the barrier, $\mathrm{d}\tau = -\mathrm{d}t''$ (see figure 1). Equivalently, the motion in the plane of imaginary coordinates is dictated by $\mathbf{k}' = -\mathrm{d}\mathbf{r}''/\mathrm{d}\tau$ and $\mathbf{F}'' = -\mathrm{d}\mathbf{k}'/\mathrm{d}\tau$. Trajectories A, B and C are depicted in figure 9. Their real parts in the classically forbidden region are almost identical because they present similar values of $\mathbf{k}''(t_i)$ and $\mathbf{F}'(t_i)$. The motion in the imaginary plane, however, is different due to the very distinct values of $\mathbf{k}''(t_i)$. Trajectory B presents $\mathbf{k}'(t_i) = 0$ and thus its motion in the complex plane is solely dictated by the imaginary value of the electric field, which barely changes its direction during tunneling. Thus, the motion in the imaginary plane occurs along a straight line. The initial values of $\mathbf{k}'$ for trajectories A and C are non zero and point in opposite directions (see figure 8). During tunneling, they are modified by $\mathbf{F}''$, giving rise to clockwise motion in trajectory A and to anti-clockwise motion in trajectory B along the plane of imaginary coordinates (see figure 9). Because of its initial angular momentum, p_+ (p_-) electrons can be driven more easily along trajectory A (B) than p_- (p_+) electrons, which leads to different recollision densities and leads to the time-dependent spin polarization in recollision.

3.2. Attosecond control of spin polarization

In this section we discuss how modifying the parameters of the driving fields can affect the degree of spin polarization of the recolliding electrons. In particular, we analyze the effect of varying the relative intensities of

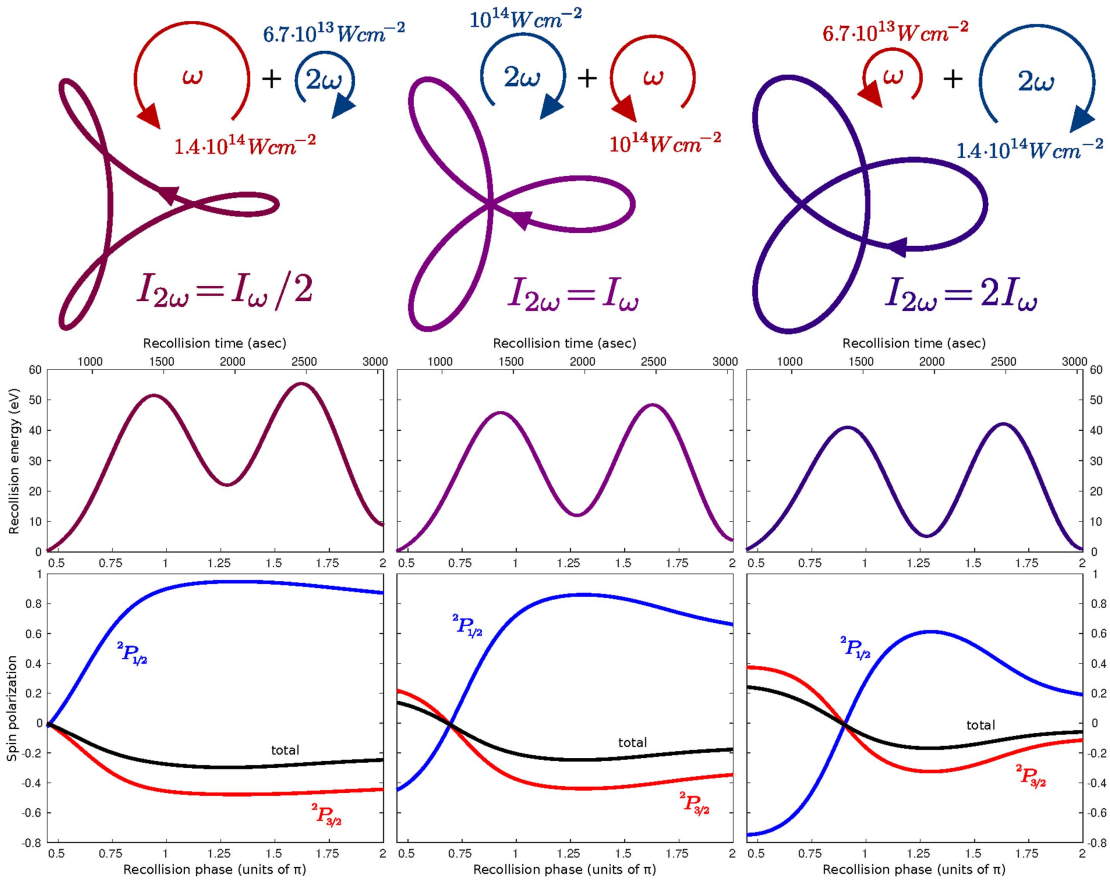

Figure 10. Attosecond control of spin polarization. Upper figures: Lissajous curves representing the electric fields resulting from combining a RCP field with frequency $\omega = 0.05$ a.u. and a LCP field with frequency 2ω with different relative intensities: $I_{2\omega} = I_\omega/2$ (left column), $I_{2\omega} = I_\omega$ (central column) and $I_{2\omega} = 2I_\omega$ (right column). The values of I_ω and $I_{2\omega}$ considered in each case are indicated in the figure. Middle panels: recollision energy as a function of the recollision time. Lower panels: spin polarization as a function of the recollision time. Results have been calculated by keeping the time of return on the real time axis.

the two counter-rotating fields. Figure 10 contains a representation of the electric fields resulting from making the intensity of the second harmonic half and twice the intensity of the fundamental field (see parameters of the fields in figure 10 and in its footnote). Increasing the relative intensity of the fundamental field shrinks the width of the field lobes. Enhancing the relative intensity of the second harmonic has the opposite effect. The corresponding recollision energy and spin polarization, obtained with these fields, are shown in 10, as a function of the recollision time, for one optical cycle of the fundamental field. For comparison purposes, the results obtained for equal intensities of the counter-rotating fields (already discussed in the previous section), are included in figure 10.

Spin polarization is presented in figure 10 (lower panels), also as a function of the recollision time. We can see that relatively small modifications of the fields intensities lead to dramatic changes in the degree of polarization, allowing to achieve a high degree of control. In particular, by tuning the relative intensities of the fields, it is possible to select the instant at which spin polarization changes it sign: increasing the intensity of the fundamental field shifts the change of sign towards earlier times, whereas increasing the intensity of its second harmonic has the opposite effect.

4. Conclusions

The possibility of inducing recollision with spin-polarized electrons opens new directions in attosecond spectroscopy. Electron spin and orbital angular momentum will play an important role in well-established recollision-driven techniques such as photoelectron diffraction and holography [32–37] or high harmonic generation [21, 23, 26, 29, 38–42]. We have shown that the use of intense two-color counter-rotating bi-circular fields can drive electron–core recollision with a degree of spin polarization that depends on the recollision time and therefore on the recollision energy.

Electron spin polarization upon tunnel ionization is intrinsically related to the generation of spin-polarized currents in the ionic core [43]. In this context, the potential of inducing recollision within one optical cycle of the driving field can allow for probing spin-polarized currents in atoms and molecules with sub-femtosecond and sub-Angstrom resolution. The time-dependence of spin polarization could be exploited to reconstruct information of the recollision process itself from spin-resolved measurements of diffracted electrons. A recolliding spin-up electron will interact differently with the ionic core if the core has spin up or spin down. Therefore, measurements of the spin of recolliding currents can provide 'snapshots' of spin-resolved dynamics in the ion between ionization and recollision.

Our work shows that the degree of spin polarization can be modified as desired by tailoring the driving fields. Changing the relative intensities of the counter-rotating fields can smoothly change the level of spin polarization of the recolliding currents, controlling its magnitude and sign as a function of recollision time and recollision energy. In particular, we have shown that one can keep the sign of spin polarization constant across the whole recollision window, or shift the point at which spin polarization changes its sign, with attosecond precision. These results open the way for attosecond control of spin-resolved dynamics in atoms and molecules.

Acknowledgments

The authors acknowledge support from the DFG grant SM 292/2-3 and from the DFG SPP 1840 'Quantum Dynamics in Tailored Intense Fields'.

References

[1] Pauli W 1925 *Z. Phys.* **31** 765
[2] Coey J M D 2010 *Magnetism and Magnetic Materials* (Cambridge: Cambridge University Press)
[3] Kessler J 1976 *Polarized Electrons* (Berlin: Springer)
[4] Fano U 1969 *Phys. Rev.* **178** 131
[5] Lambropoulos P 1976 *Adv. At. Mol. Phys.* **12** 87
[6] Dixit S N, Lambropoulos P and Zoller P 1981 *Phys. Rev.* A **24** 318
[7] Nakajima T and Lambropoulos P 2002 *Europhys. Lett.* **57** 25
[8] Barth I and Smirnova O 2013 *Phys. Rev.* A **88** 013401
[9] Milošević D B 2016 *Phys. Rev.* A **93** 051402
[10] Hartung A *et al* 2016 *Nat. Photon.* **10** 526
[11] Barth I and Smirnova O 2011 *Phys. Rev.* A **84** 063415
[12] Herath T, Yan L, Lee S K and Li W 2012 *Phys. Rev. Lett.* **109** 043004
[13] Barth I and Smirnova O 2013 *Phys. Rev.* A **87** 013433
[14] Barth I and Smirnova O 2013 *Phys. Rev.* A **87** 065401
[15] Barth I and Lein M 2014 *J. Phys. B: At. Mol. Opt. Phys.* **47** 204016
[16] Kaushal J, Morales F and Smirnova O 2015 *Phys. Rev.* A **92** 063405
[17] Liu K and Barth I 2016 *Phys. Rev.* A **94** 043402
[18] Yudin G L and Ivanov M Y 2001 *Phys. Rev.* A **64** 035401
[19] Eichmann H, Egbert A, Nolte S, Momma C, Wellegehausen B, Becker W, Long S and McIver J K 1995 *Phys. Rev.* A **51** R3414
[20] Long S, Becker W and McIver J K 1995 *Phys. Rev.* A **52** 2262
[21] Milošević D B, Becker W and Kopold R 2000 *Phys. Rev.* A **61** 063403
[22] Milošević D B 2015 *Opt. Lett.* **40** 2381
[23] Medišauskas L, Wragg J, van der Hart H and Ivanov M Y 2015 *Phys. Rev. Lett.* **115** 153001
[24] Zuo T and Bandrauk A D 1995 *J. Nonlinear Opt. Phys. Mater.* **04** 533
[25] Ivanov M and Pisanty E 2014 *Nat. Photon.* **8** 501
[26] Kfir O *et al* 2015 *Nat. Photon.* **9** 99
[27] Mauger F, Bandrauk A D and Uzer T 2016 *J. Phys. B: At. Mol. Opt. Phys.* **49** 10LT01
[28] Bandrauk A D, Mauger F and Yuan K-J 2016 *J. Phys. B: At. Mol. Opt. Phys.* **49** 23LT01
[29] Smirnova O, Mairesse Y and Patchkovskii S 2015 *J. Phys. B: At. Mol. Opt. Phys.* **48** 234005
[30] Baykusheva D, Ahsan M S, Lin N and Wörner H J 2016 *Phys. Rev. Lett.* **116** 123001
[31] Smirnova O and Ivanov M 2014 Multielectron high harmonic generation: simple man on a complex plane *Attosecond and XUV Physics* ed T Schultz and M Vrakking (Hoboken, NJ: Wiley-VCH) ch 7 pp 201–56
[32] Spanner M, Smirnova O, Corkum P B and Ivanov M Y 2004 *J. Phys. B: At. Mol. Opt. Phys.* **37** L243
[33] Meckel M *et al* 2008 *Science* **320** 1478
[34] Huismans Y *et al* 2011 *Science* **331** 61
[35] Blaga C I, Xu J, DiChiara A D, Sistrunk E, Zhang K, Agostini P, Miller T A, DiMauro L F and Lin C D 2012 *Nature* **483** 194
[36] Meckel M, Staudte S, Patchkovskii A, Villeneuve D M, Corkum P B, Dorner R and Spanner M 2014 *Nat. Phys.* **10** 594
[37] Pullen M G *et al* 2015 *Nat. Commun.* **6** 7262
[38] Milošević D B and Becker W 2000 *Phys. Rev.* A **62** 011403
[39] Wörner H J *et al* 2011 *Science* **334** 208
[40] Fleischer A, Kfir O, Diskin T, Sidorenko P and Cohen O 2014 *Nat. Photon.* **8** 543
[41] Pisanty E, Sukiasyan S and Ivanov M 2014 *Phys. Rev.* A **90** 043829
[42] Cireasa R *et al* 2015 *Nat. Phys.* **11** 654
[43] Barth I and Smirnova O 2014 *J. Phys. B: At. Mol. Opt. Phys.* **47** 204020
[44] Odžak S, Hasović E, Becker W and Milošević D B 2017 Atomic processes in bicircular fields *J. Mod. Opt.* **64** 971–80
[45] Hasović E, Odžak S, Becker W and Milošević D B 2016 High-order harmonic generation in non-planar molecules driven by a bicircular field *Mol. Phys.* (https://doi.org/10.1080/00268976.2016.1257830)